PHYSICAL REVIEW B **92**, 140404(R) (2015)

Magnons in tetragonal CuO

S. Moser,[1,*] N. E. Shaik,[1] D. Samal,[2,3] S. Fatale,[1] B. Dalla Piazza,[1] M. Dantz,[4] J. Pelliciari,[4] P. Olalde-Velasco,[4] T. Schmitt,[4] G. Koster,[2] F. Mila,[5] H. M. Rønnow,[1] and M. Grioni[1]

[1]*Institute of Condensed Matter Physics (ICMP), Ecole Polytechnique Fédérale de Lausanne (EPFL), CH-1015 Lausanne, Switzerland*

[2]*MESA+ Institute for Nanotechnology, University of Twente, P.O. Box 217, 7500AE Enschede, The Netherlands*

[3]*Max Planck Institute for Solid State Research, DE-70569 Stuttgart, Germany*

[4]*Swiss Light Source, Paul Scherrer Institut, CH-5232 Villigen PSI, Switzerland*

[5]*Institute of Theoretical Physics (ITP), Ecole Polytechnique Fédérale de Lausanne (EPFL), CH-1015 Lausanne, Switzerland*

(Received 15 July 2015; published 6 October 2015)

We investigate by resonant inelastic x-ray scattering the magnetic excitations in thin films of tetragonal CuO. We identify a spin wave excitation, dispersing on two cupratelike antiferromagnetic sublattices. Its energy at the boundary of the Brillouin zone (220 meV), is significantly lower than typical values ($E \sim 300$ meV) found in two-dimensional cuprates. A spin wave expansion starting from an extended Hubbard model suggests two possible scenarios for this energy lowering.

DOI: 10.1103/PhysRevB.92.140404 PACS number(s): 74.72.Cj, 74.25.Jb, 75.30.Ds, 78.70.Ck

Magnetism in the undoped, insulating quasi-two-dimensional (2D) cuprates is determined by the 180° Cu-O-Cu bonds of their corner-sharing copper oxide layers [Fig. 1(a)]. The resulting large superexchange interaction $J \sim 130$ meV [1] yields antiferromagnetic (AFM) ground states with ordering temperatures $T_N \sim 300$ K in materials such as $Sr_2CuO_2Cl_2$ (SCOC) [2] or La_2CuO_4 (LCO) [3]. Phenomenologically, these systems can be described by extended spin-1/2 Heisenberg models with antiferromagnetic coupling on a square lattice [4,5], in agreement with second-order superexchange theory. However, to make contact with other spectroscopies one needs to adopt a more microscopic description in terms of an extended Hubbard model. To be quantitative, it is necessary to go beyond second-order perturbation theory and to consider the effective spin model generated by the one-band Hubbard model up to fourth order in hopping. Such a procedure renormalizes the two-spin interactions and also leads to four-spin interactions. This approach yields more realistic values for the on-site Coulomb repulsion U, is consistent with higher-energy resonant inelastic x-ray scattering (RIXS) and angle-resolved photoemission spectroscopy (ARPES) data, and provides good fits to the experimentally observed spin excitation spectra [6,7].

A recent exciting development was the discovery of a new tetragonal form of the simple binary oxide CuO, with an alternative structure to that of the cuprates. Tetragonal CuO (T-CuO) can be grown epitaxially on a $SrTiO_3$ (001) substrate up to a thickness of several unit cells [8–10]. In this material CuO_6 octahedra give rise to infinite CuO layers, consisting of edge-sharing CuO_4 plaquettes, stacked along the c axis. At variance with the CuO_2 cuprate layers, oxygen ions do not bridge nearest-neighbor (NN) but next-NN copper ions. Electronically, the edge-sharing structure is well described by two interpenetrating corner-sharing sublattices [Fig. 1(b)], with lattice parameters typical of cuprates and 180° Cu-O-Cu bonds, coupled by an intersublattice hopping term $t_d \sim -t/4$ [11].

Magnetically the situation is not yet as clear. The second sublattice is expected to introduce a small but finite intersublattice exchange term J_d. Because of the additional 90° Cu-O-Cu bonds, the coupling could be either ferromagnetic or antiferromagnetic but, in any case, it introduces frustration. In the classical limit, the system would still develop independent AFM Heisenberg order on each sublattice. However, if quantum fluctuations are taken into account, J_d is expected to lock the relative orientation of the two sublattices and to break the fourfold rotational C_4 symmetry, leading to an additional Ising order parameter [12–14].

To examine these speculations, we have studied the magnetic excitation spectrum of T-CuO. Since inelastic neutron scattering is inadequate due to the limited film thickness, we employ RIXS at the Cu L_3 (Cu $2p_{3/2} \rightarrow 3d$) edge [15]. We find a magnon excitation, dispersing with the same symmetry as the typical magnon excitations of the cuprate parent compounds, indicative of AFM correlations on each sublattice. The zone boundary magnon energy (220 meV) is significantly reduced from typical cuprate values of ∼300 meV. A spin wave expansion starting from an extended Hubbard model provides two qualitatively different scenarios for this energy lowering. We further demonstrate that magnetic couplings up to the fifth neighbor need to be taken into account to accurately describe the spin wave dispersion in an effective model. This is in line with standard cuprates, since the fifth neighbor in the CuO plane is the third neighbor on a given sublattice.

Measurements were performed with the SAXES spectrometer of the ADRESS beam line at the Swiss Light Source (SLS), Paul Scherrer Institut [16]. Thin films (6 unit cells) of T-CuO were grown ex situ by pulsed laser deposition on Nb-doped $SrTiO_3$ (001) substrates and characterized by reflection high-energy electron diffraction [10]. Here we show RIXS data collected at $T = 20$ K from two samples mounted with either the (100) or the (110) direction in the horizontal scattering plane. The scattering angle was 130°, and the incoming light was polarized perpendicular (σ) to the plane [17]. Data taken with π polarization are similar, but suffer from a large linear dichroism in absorption. The total transferred momentum was $|\vec{q}| \sim 0.85$ Å^{-1} at 931 eV photon energy. By rotating the sample around the vertical axis, its projection q on the

*Corresponding author: simon.moser@epfl.ch

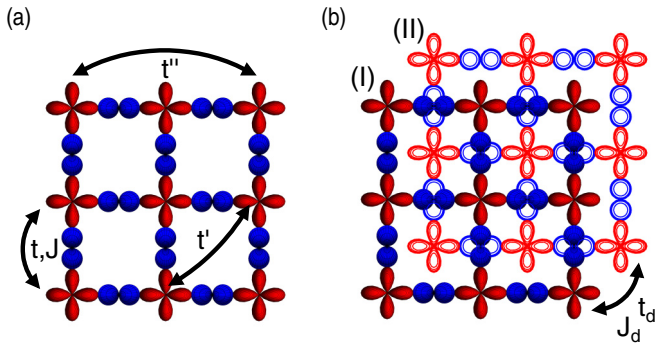

FIG. 1. (Color online) Corner-sharing CuO_2 (a) and edge-sharing CuO (b) layers. Red and blue contours indicate Cu $d_{x^2-y^2}$ and O p_x/p_y orbitals, respectively. The CuO layer is seen as the superposition of two corner-sharing sublattices (I) and (II). The effective hopping terms are indicated by arrows. Additionally, we mark the effective exchange terms of the J_1-J_2 model.

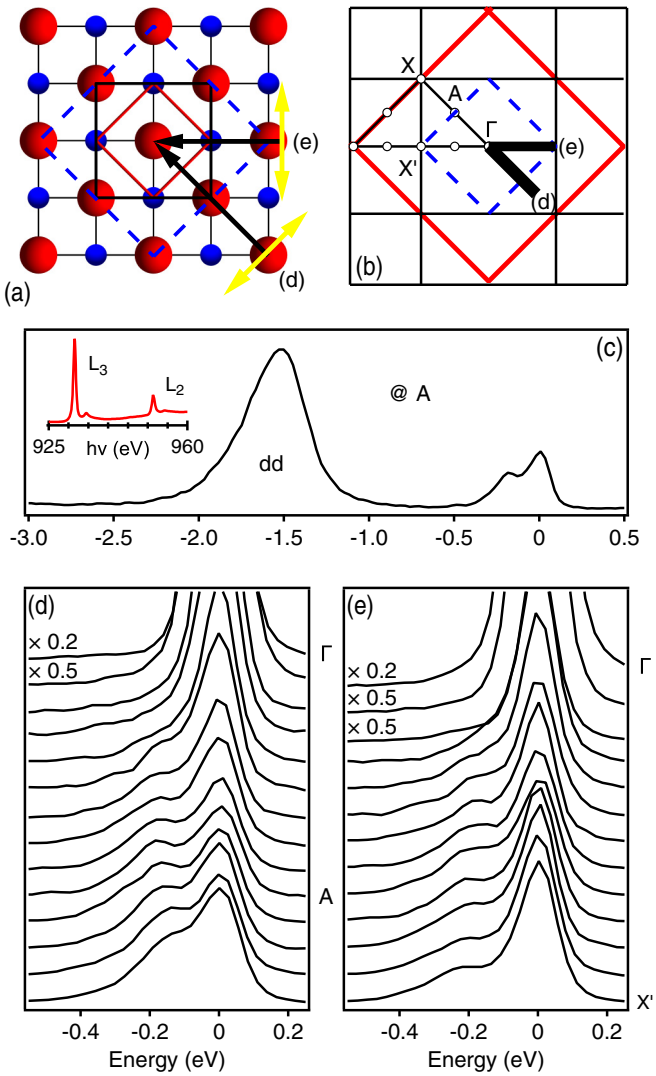

FIG. 2. (Color online) (a) The structure of a CuO layer, with Cu (O) ions indicated in red (blue). The red square is the unit cell. The (blue dashed) black square is the (magnetic) unit cell of one sublattice. The corresponding Brillouin zones are shown in (b). (c) RIXS spectrum taken at the A point, on the magnetic BZ boundary. The inset shows the Cu $L_{2,3}$ x-ray absorption spectrum. (d), (e) Cu L_3 RIXS spectra measured along the ΓX (d) and $\Gamma X'$ (e) high-symmetry directions. The light polarization and momentum ranges are shown by yellow arrows in (a) and by thick black lines in (b), respectively.

ab plane was varied between 0 (specular geometry) and 0.73 $Å^{-1} = 0.92\pi/a$ (grazing incidence). Self-absorption is negligible over the whole range. The total energy resolution, determined from the elastic peak measured on a coplanar polycrystalline carbon sample, was $\Delta E = 125$ meV.

In Fig. 2(a) the red square is the primitive unit cell of the CuO plane (unprimed labels). The black square is the primitive cell of a corner-sharing cuprate sublattice (primed labels), and the blue dashed square its magnetic unit cell. The corresponding Brillouin zones (BZ) are shown in Fig. 2(b), where thick lines indicate the momentum range covered by the experiment along the two high-symmetry directions. Panel 2(c) shows a representative RIXS spectrum. The prominent dd manifold centered at -1.5 eV contains excitations from the single Cu $3d_{x^2-y^2}$ hole state to d_{z^2}, d_{xy}, and $d_{xz/yz}$ orbitals [18]. A Gaussian fit (not shown) yields the tetragonal crystal field parameters $10Dq \sim 1.5 \pm 0.1$ eV, $Dt \sim 0.13 \pm 0.03$ eV, and $Ds \sim 0.25 \pm 0.05$ eV. The $10Dq$ and Dt values are typical of 2D cuprates such as SCOC [18]. This already suggests that the in-plane electronic and magnetic structure of one T-CuO sublattice should thus be fairly comparable to those of a typical cuprate layer. Ds is 25% smaller than in SCOC, consistent with the smaller tetragonal elongation of T-CuO (T-CuO: $c/a \sim 1.5$; SCOC: $c/a \to \infty$). At lower energy, the elastic peak exhibits a pronounced shoulder at ~ -0.2 eV which, by analogy with the cuprates, is assigned to a spin excitation.

The momentum dependence of the low-energy response is illustrated in Figs. 2(d) for the ΓX and 2(e) for the $\Gamma X'$ directions. As common practice in cuprates, all spectra are normalized to the integrated intensity of the dd manifold. The low-energy shoulder disperses along both directions from a maximum of $\sim$220 meV, and merges with a growing elastic peak near Γ. For a quantitative analysis, we subtract from the raw data scaled versions of the spectrum measured at Γ, representing the elastic and phonon scattering. The second derivative of the difference spectra is shown for both high-symmetry directions in the intensity plot of Fig. 3(a), where the magnon dispersion is now clearly identified. The figure also shows data for SCOC [7], as a typical cuprate reference. Remarkably, the magnon dispersion in T-CuO follows the overall symmetry of the SCOC dispersion. This strongly suggests that the magnetic Brillouin zones for both the edge-sharing T-CuO and the corner-sharing SCOC are essentially identical, and that the magnon preferentially moves on two independent corner-sharing sublattices. It further proves the AFM spin correlation on each sublattice of T-CuO, a central result of this work. Compared to SCOC or other typical insulating cuprates, however, the magnon energy is reduced by as much as 30% [19,20].

In order to model the data, we start—in analogy to the cuprates—from the extended Hubbard model on a square lattice [4–6] with effective on-site Hubbard U, NN hopping

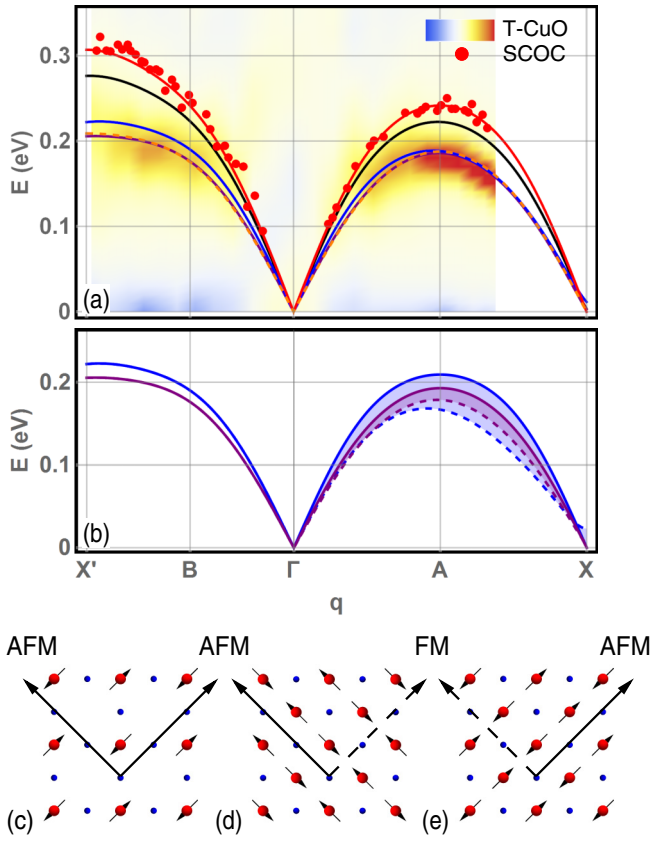

FIG. 3. (Color online) (a) Second derivative map extracted from the data of Fig. 2. Data for SCOC [7] are shown as red circles. The lines are t-t'-t''-U-Hubbard model fits to the data: (red) SCOC, (black) SCOC + $t_d = 100$ meV, (orange) parameter set (i), (blue) parameter set (ii), and (purple) parameter set (iii) of Table I. The average of the two possible columnar orderings is plotted. (b) Band dispersion corresponding to parameter set (ii) (blue) and (iii) (purple). Solid (dashed) lines refer to the branch along the AFM (FM) direction. (c)–(e) Magnetic structures: independent sublattice model (c); columnar ordering with FM direction along (1,1) (d) and (−1,1) (e).

t, and further hopping terms t' and t''. We derive the spin Hamiltonian from this model up to fourth order in the hopping parameters and perform a spin wave expansion for AFM ordering on each sublattice [Fig. 3(c)] [20]. The red curve shows a fit to the SCOC data with parameters $U = 3.5$ eV, $t = 490$ meV, $t' = -200$ meV, and $t'' = 75$ meV, as obtained in Ref. [20]. To model the T-CuO data, we first assume independent magnon dynamics on each CuO_2 sublattice. Whereas a variation of U does not yield satisfying results within reasonable boundaries, a significantly lowered $t \to 425$ meV mimics the dispersion [orange dashed, (i)]. As J scales with t^2, this would correspond to a significant reduction of the superexchange interaction of 76% with respect to SCOC as a consequence of its different geometry.

As ARPES finds a significant coupling between sublattices [11], we further study the effect of $t_d \sim 100$ meV on the magnon dispersion. Even if the magnetic properties are still expected to be dominated by J, t_d will introduce a small but finite exchange term J_d between sublattices. If only the terms of the Hamiltonian quadratic in spin matrices and

TABLE I. Fit parameters of the magnon dispersion of SCOC, and of T-CuO obtained by (i) varying t, (ii) introducing t_d, and (iii) varying t and introducing t_d.

	t_d (meV)	t (meV)	t' (meV)	t'' (meV)	U (eV)
SCOC	0	490	–200	75	3.5
(i)	0	425	–200	75	3.5
(ii)	167	490	–200	75	3.5
(iii)	100	440	–200	75	3.5

nearest-neighbor couplings are considered, this model becomes the well-known J_1-J_2 model with $J_2 \equiv J > J_1 \equiv J_d$. The lattice will be fully frustrated and quantum fluctuations will favor a parallel spin alignment between individual sublattices (columnar ordering) [13,21]. Upon inclusion of the fourth-order terms in spin matrices, an additional contribution to the Hamiltonian appears, which conversely favors a perpendicular spin alignment [10]. These terms, however, are dominated by quantum fluctuations, and the system is again expected to adapt columnar order: the C_4 symmetry is broken and the system orders ferromagnetic (FM) along $(\pm 1, 1)$, while it orders AFM along $(\mp 1, 1)$ [Figs. 3(d) and 3(e)]. This lifts the magnon degeneracy along ΓX and produces two magnon branches which are simultaneously measured by RIXS.

To see the trend of nonzero intersublattice coupling t_d, we first keep U, t, t', and t'' at the SCOC values and include an additional $t_d = 100$ meV estimated by ARPES [10,11]. The result is the black solid curve in Fig. 3(a). Along ΓX we plot the average of the dispersion along the two possible columnar orientations (d) and (e). Clearly, t_d leads to an overall reduction of the magnon dispersion, qualitatively reproducing the experimental trend. However, to obtain quantitative agreement t_d needs to be further increased to $t_d \to 167$ meV [blue, (ii)]. A more realistic approach takes into account both a reduction of t and a nonzero t_d. For example, satisfactory results can be obtained for $t = 440$ meV and $t_d = 100$ meV [purple, (iii)]. A summary of the fit parameters used in this work is given in Table I.

Figure 3(b) separately shows the two magnon branches along ΓX for fit parameter sets [(ii), blue] and [(iii), purple], respectively. Solid lines mark the solution along the AFM direction, and dashed lines the solution along the FM direction. Clearly, the energy difference between the two ordering directions is governed by t_d. The magnon energy is more strongly reduced along the FM direction. The complexity of the dispersion relation, however, hides the intuitive physical origin of this discrepancy [10].

To identify the responsible interaction terms among the complex interference pattern of closed hopping loops, we calculate the effective Heisenberg-like exchange coupling terms J_1-J_5 of the first five neighbors as defined in the inset of Fig. 4 (further couplings are negligible and are not shown) [20]. These include the contribution of the quartic plaquette terms (see Ref. [10]), which gives a negative (positive) contribution along the AFM (FM) direction. The calculation is done in two steps: (i) derive the effective model to fourth order, which gives an effective spin Hamiltonian that still has all the spatial symmetries of the original Hubbard model; (ii) decouple the

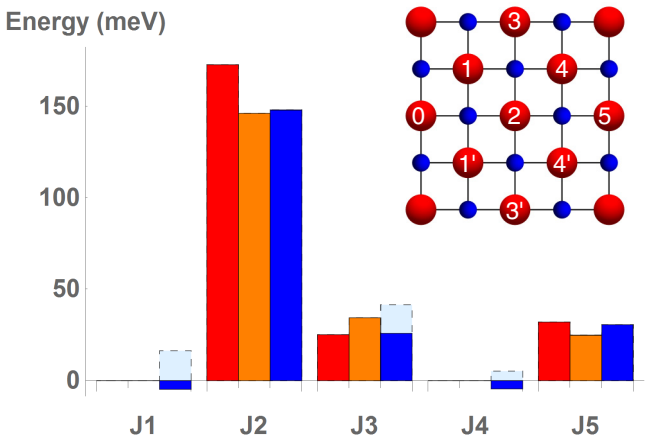

FIG. 4. (Color online) Effective exchange interaction terms of the first five nearest neighbors, calculated for SCOC (red), and with parameter sets (i) (orange) and (ii) (blue) of Table I, respectively. Dark blue corresponds to the AFM direction, and light blue to the FM direction. Inset: Definition of the effective exchange interaction terms on the T-CuO lattice (red: copper; blue: oxygen). Primed (unprimed) numbers correspond to the AFM (FM) direction of the columnar phase.

four-spin terms assuming collinear order (which is known to be stabilized by quantum fluctuations), which leads to different effective exchange coupling along AFM (primed numbers) and FM (unprimed numbers) ordering directions. The red bars show the results for SCOC. The orange bars are the results for parameter set (i), i.e., the independent sublattice model with a reduced $t = 425$ meV. The blue bars show results for the SCOC parameters and an additional intersublattice coupling $t_d = 167$ meV (ii). Dark (light) blue corresponds to exchange couplings along the AFM (FM) direction.

In all cases the main source of interaction is $J_2 \equiv J$, which largely determines the magnon energy and forces AFM ordering on each sublattice. A reduction of t has a similar effect as the introduction of t_d, as it significantly decreases J_2. The intersublattice coupling t_d, however, introduces effective exchange terms $J_1 \equiv J_d$ and J_4. The latter directly compete with J_2, but are too small to influence the magnon significantly along the AFM direction. Along the FM direction the frustration is clearly enhanced as J_1 and J_3 considerably gain weight. This effectively reduces the magnon energy. As the higher-order NN exchange terms enter the magnon dispersion in a nonlinear way, all J terms are needed to describe the spin wave dispersion in an effective model [10]. A simple J_1-J_2 model thus seems rather inappropriate to describe magnetism in T-CuO. Finally, it is interesting to note that the multimagnon continuum typically observed, e.g., in SCOC and LCO is particularly weak in T-CuO.

To date, the energy resolution of state-of-the art RIXS experiments cannot distinguish between the independent-sublattice, the columnar, or alternative models. ARPES data, however, favors the columnar lattice model as the most compatible solution. Such an ordering might give rise to a small ferromagnetic moment along the $(\pm 1, 1)$ directions, and to observable x-ray magnetic circular dichroism in T-CuO. It would equally give rise to inequivalent Bragg conditions along $(\pm 1, 1)$, which may be exploited in resonant elastic x-ray scattering experiments. We leave these ideas for a future study.

In summary, we have employed RIXS to obtain qualitative and quantitative new insight into the magnetic excitation spectrum of the edge-sharing two-dimensional cuprate T-CuO. Measuring the full spin-wave spectrum, we found a magnon, essentially dispersing on two AFM ordered sublattices. The magnon energy is significantly lower than typical values for the corner-sharing 2D cuprate compounds. The observed magnon dispersion can be described by an extended t-U-Hubbard model on each sublattice, with or without taking into account the coupling between them. We have shown the difference between both cases, and provided parameters that satisfactorily explain our data.

The SAXES instrument at the ADRESS beam line of the Swiss Light Source was jointly built by Paul Scherrer Institut, EPFL, and Politecnico di Milano. We acknowledge support by the Swiss National Science Foundation. J.P. and T.S. acknowledge financial support by the Dysenos AG, by Kabelwerke Brugg AG Holding, the Fachhochschule Nordwestschweiz, and the Paul Scherrer Institut. We thank Mona Berciu for valuable discussions.

[1] P. W. Anderson, Phys. Rev. **79**, 350 (1950); J. B. Goodenough, *ibid.* **100**, 564 (1955); J. Phys. Chem. Solids **6**, 287 (1958); J. Kanamori, *ibid.* **10**, 87 (1959).

[2] M. Greven, R. J. Birgeneau, Y. Endoh, M. A. Kastner, M. Matsuda, and G. Shirane, Z. Phys. B **96**, 465 (1995).

[3] M. A. Kastner, R. J. Birgeneau, G. Shirane, and Y. Endoh, Rev. Mod. Phys. **70**, 897 (1998).

[4] For a review, see E. Manousakis, Rev. Mod. Phys. **63**, 1 (1991).

[5] R. Coldea, S. M. Hayden, G. Aeppli, T. G. Perring, C. D. Frost, T. E. Mason, S.-W. Cheong, and Z. Fisk, Phys. Rev. Lett. **86**, 5377 (2001).

[6] J.-Y. P. Delannoy, M. J. P. Gingras, P. C. W. Holdsworth, and A.-M. S. Tremblay, Phys. Rev. B **79**, 235130 (2009).

[7] M. Guarise, B. Dalla Piazza, M. Moretti Sala, G. Ghiringhelli, L. Braicovich, H. Berger, J. N. Hancock, D. van der Marel, T. Schmitt, V. N. Strocov, L. J. P. Ament, J. van den Brink, P.-H. Lin, P. Xu, H. M. Rønnow, and M. Grioni, Phys. Rev. Lett. **105**, 157006 (2010).

[8] W. Siemons, G. Koster, D. H. A. Blank, R. H. Hammond, T. H. Geballe, and M. R. Beasley, Phys. Rev. B **79**, 195122 (2009).

[9] D. Samal, H. Tan, Y. Takamura, W. Siemons, J. Verbeeck, G. Van Tendeloo, E. Arenholz, C. A. Jenkins, G. Rijnders, and Gertjan Koster, Eurphys. Lett. **105**, 17003 (2014).

[10] See Supplemental Material at http://link.aps.org/supplemental/10.1103/PhysRevB.92.140404 for more details.

[11] S. Moser, L. Moreschini, H.-Y. Yang, D. Innocenti, F. Fuchs, N. H. Hansen, Y. J. Chang, K. S. Kim, A. L. Walter, A. Bostwick,

E. Rotenberg, F. Mila, and M. Grioni, Phys. Rev. Lett. **113**, 187001 (2014).

[12] C. L. Henley, Phys. Rev. Lett. **62**, 2056 (1989).

[13] P. Chandra, P. Coleman, and A. I. Larkin, Phys. Rev. Lett. **64**, 88 (1990).

[14] C. Weber, L. Capriotti, G. Misguich, F. Becca, M. Elhajal, and F. Mila, Phys. Rev. Lett. **91**, 177202 (2003).

[15] L. J. P. Ament, M. van Veenendaal, T. P. Devereaux, J. P. Hill, and J. van den Brink, Rev. Mod. Phys. **83**, 705 (2011).

[16] V. N. Strocov, T. Schmitt, U. Flechsig, T. Schmidt, A. Imhof, Q. Chen, J. Raabe, R. Betemps, D. Zimoch, J. Krempasky, X. Wang, M. Grioni, A. Piazzalunga, and L. Patthey, J. Synchrotron Radiat. **17**, 631 (2010); G. Ghiringhelli, A. Piazzalunga, C. Dallera, G. Trezzi, L. Braicovich, T. Schmitt, V. N. Strocov, R. Betemps, L. Patthey, X. Wang, and M. Grioni, Rev. Sci. Instrum. **77**, 113108 (2006).

[17] L. J. P. Ament, G. Ghiringhelli, M. M. Sala, L. Braicovich, and J. van den Brink, Phys. Rev. Lett. **103**, 117003 (2009).

[18] M. Moretti Sala, V. Bisogni, C. Aruta, G. Balestrino, H. Berger, N. B. Brookes, G. M. de Luca, D. Di Castro, M. Grioni, M. Guarise, P. G. Medaglia, F. Miletto Granozio, M. Minola, P. Perna, M. Radovic, M. Salluzzo, T. Schmitt, K. J. Zhou, L. Braicovich, and G. Ghiringhelli, New J. Phys. **13**, 043026 (2011).

[19] L. Braicovich, L. J. P. Ament, V. Bisogni, F. Forte, C. Aruta, G. Balestrino, N. B. Brookes, G. M. De Luca, P. G. Medaglia, F. Miletto Granozio, M. Radovic, M. Salluzzo, J. van den Brink, and G. Ghiringhelli, Phys. Rev. Lett. **102**, 167401 (2009).

[20] B. Dalla Piazza, M. Mourigal, M. Guarise, H. Berger, T. Schmitt, K. J. Zhou, M. Grioni, and H. M. Rønnow, Phys. Rev. B **85**, 100508(R) (2012).

[21] R. R. P. Singh, W. Zheng, J. Oitmaa, O. P. Sushkov, and C. J. Hamer, Phys. Rev. Lett. **91**, 017201 (2003).